Negative refraction and focusing of ultrasound in two-dimensional phononic crystals

Alexey Sukhovich,[1] Li Jing,[2] and John H. Page[1]
[1]*Department of Physics and Astronomy, University of Manitoba, Winnipeg, Manitoba, Canada R3T 2N2*
[2]*Department of Physics, Wuhan University, Wuhan 430072, People's Republic of China*
(Received 30 August 2007; published 16 January 2008)

We present experimental demonstrations of negative refraction and focusing of ultrasonic waves in two-dimensional phononic crystals made of stainless steel rods assembled in a triangular lattice and immersed in a liquid. Negative refraction is achieved for the range of frequencies in the second band, where the directions of the wave vector and group velocity are antiparallel to each other due to circular equifrequency contours. Negative refraction is unambiguously observed using a prism-shaped crystal. By exploiting the circular equifrequency contours in the second band, focusing of the ultrasonic field emitted by a pointlike source was demonstrated using a flat phononic crystal filled with and immersed in water. During these experiments, the importance of imaging in the regime of all angle negative refraction (AANR) was established for obtaining high-quality images. The regime of AANR was achieved in a similar flat crystal, in which the liquid inside the crystal (methanol) was different from the outside medium (water). This design resulted in matching circular equifrequency contours at the frequency of 0.55 MHz, implying that a flat ultrasonic lens with an effective refractive index of −1 was realized. By imaging a subwavelength line source with this crystal, a resolution of 0.55λ was observed, which is just above the diffraction limit.

DOI: 10.1103/PhysRevB.77.014301 PACS number(s): 43.35.+d, 63.20.−e

I. INTRODUCTION

In 1964 Victor Veselago studied theoretically the properties of, then hypothetical, materials with both electric permittivity ε and magnetic permeability μ simultaneously negative. He called them left-handed (LH) materials, as opposed to regular right-handed (RH) materials that have both ε and μ positive.[1] In the case of negative ε and μ, causality forces a negative sign to be ascribed to the refractive index n of a LH material,[2] which in turn implies that an electromagnetic wave propagating in such medium will have its Poynting vector $\vec{S}$ and wave vector $\vec{k}$ pointing in opposite directions. As a result, LH materials exhibit many unusual properties, one of them being *negative* refraction, which takes place when an electromagnetic wave crosses the boundary between LH and RH materials. Negative refraction was first demonstrated experimentally in left-handed metamaterials, which are artificial structures with *effective* negative ε and μ in a certain frequency range.[3]

Bending of light "in the wrong way" can also be achieved with the help of photonic crystals.[4] In this case, both ε and μ are locally positive everywhere inside the crystal, and negative refraction is achieved because of crystal anisotropy. The direction of light propagation inside a photonic crystal is given by the gradient vector $\nabla_{\vec{k}}\omega(\vec{k})$ and thus is defined by the shape of the crystal equifrequency contour or surface. Negative refraction was demonstrated experimentally in two-dimensional (2D) photonic crystals by employing equifrequency contours in the first[5] and second[6] bands. Negative refraction also enables a slab of a LH material to focus radiation emitted by a point source, thus acting as a flat lens.[1] The possibility of imaging with flat photonic crystals was predicted theoretically[7] and then demonstrated experimentally for both 2D and 3D crystals.[8,9]

Up to the present moment, there have been relatively few experimental studies of similar phenomena in *phononic* crystals, which are acoustic or elastic analogs of photonic crystals. Three years ago, Yang *et al.*[10] demonstrated the focusing of ultrasonic waves by a 3D phononic crystal, in which they observed a far-field image with a focal spot about five wavelengths wide. More recently, Ke *et al.*[11] studied 2D phononic crystals made of stainless steel rods assembled in a triangular crystal lattice and immersed in water. To achieve negative refraction, they employed circular equifrequency contours in the second band. Negative refraction was demonstrated by monitoring the transverse displacement of the sound beam transmitted through a flat phononic crystal with respect to the incident beam. Ke *et al.* also investigated the focusing properties of a flat crystal. As a point source, they employed the focal spot of a commercially available ultrasound focusing transducer. Ke *et al.* observed the formation of the far-field image on the output side of the crystal. The lateral resolution was found to be a couple of wavelengths. In another type of experiment, Hu *et al.*[12] observed the focusing of waves propagating on the surface of a liquid layer after the waves had passed through a square lattice of copper rods that were placed in the liquid.

In this paper, we present a direct experimental demonstration of negative refraction of ultrasound waves in a 2D prism-shaped phononic crystal. Negative refraction is achieved in the second band of the crystal, which has circular equifrequency contours over a wide frequency range, as predicted by the multiple scattering theory[13] (MST). The observed refraction angles are in excellent agreement with those predicted by the MST and Snell's law. We also observed focusing of the fields emitted by several point sources using a flat phononic crystal. High quality images were found to form on the output side of the crystal, with a resolution just above the diffraction limit at the frequency for which the all angle negative refraction (AANR) regime is valid. This resolution is much better than the focal spot width that can be achieved with conventional focusing transducers.

II. SAMPLES AND EXPERIMENTS

Our 2D phononic crystals were made of 1.02-mm-diameter stainless steel rods, which were assembled in a triangular crystal lattice with a lattice constant $a=1.27$ mm. These parameters resulted in a filling ratio of 58.4%. For negative refraction experiments, we made a phononic crystal in the shape of a right-angle prism, with the two other angles being 30° and 60°. Two sides (shortest and longest) of the prism-shaped crystal were perpendicular to the ΓM direction, while the third side was perpendicular to the ΓK direction. In imaging experiments, we employed a rectangular-shaped flat phononic crystal, which consisted of six layers stacked in the ΓM direction. Each layer had 60 rods, which ensured that the width of the crystal was much larger than its thickness and ruled out possible complications due to the edge effects.

The experiments were conducted in a water tank at frequencies up to 1.5 MHz, with (in almost all cases) the space between the rods also filled with water. In the negative refraction experiments, narrow Gaussian ultrasound pulses were generated by a 25-mm-diameter flat circular immersion transducer commercially produced by Panametrics. The input pulse was incident normally on the shortest side of the prism-shaped crystal. The field on the output side of the crystal was detected with a miniature hydrophone, which is an ultrasound detector with an active element diameter smaller than the wavelength of ultrasound in water at the frequency of the experiment. The hydrophone was attached to a 3D motorized translation stage controlled by a computer. By moving the hydrophone in a rectangular grid, we were able to scan the spatiotemporal distribution of the output field. By reading the magnitude of each recorded pulse at a particular moment of time, we were able to produce a snapshot of the outgoing field. The time evolution of the outgoing pulses was conveniently displayed by combining a sequence of snapshots taken at regular intervals of time to create a video, thereby facilitating the visualization of the wave phenomena under investigation. By digitally filtering output pulses recorded at each grid point with a narrow Gaussian bandwidth, we were able to investigate frequency dependence of the outgoing field patterns.

In focusing experiments, we used two different sound generators. The first one was a small circular transducer, a Valpey-Fisher pinducer, with an effective diameter of 2.2 mm, which was determined experimentally from the emitted field pattern. The second one was a custom-built transducer in the shape of a thin strip, which was a true subwavelength line source, since its width was about $\lambda/5$ at the design frequency (0.55 MHz). The output field was again scanned with the help of the hydrophone. A map of the field amplitude at a certain frequency was produced by Fourier transforming each acquired pulse and reading the FT amplitudes at the frequency of interest.

According to the band structure calculated by the MST, our crystals possess a stop band along the ΓM direction extending from 0.52 to 0.68 MHz, as well as a complete band gap in the range of frequencies between 1.04 and 1.18 MHz. This was verified in the transmission experiment, in which the input pulse was incident normally on the rectangular-shaped flat crystal. By measuring the cumulative phase difference between the Fourier transforms (FTs) of the transmitted and the input pulses as a function of frequency, the dispersion curve of the crystal along the ΓM direction was extracted. The dispersion curve along the ΓK direction was measured in a similar transmission experiment (a crystal with a normal along the ΓK direction was obtained from a prism-shaped one by temporarily removing the required number of rods). By folding the measured dispersion curves back into the first Brillouin zone, the experimentally accessible parts of the band structure were found. As shown in Fig. 1, an excellent agreement is observed between theory and experiment.

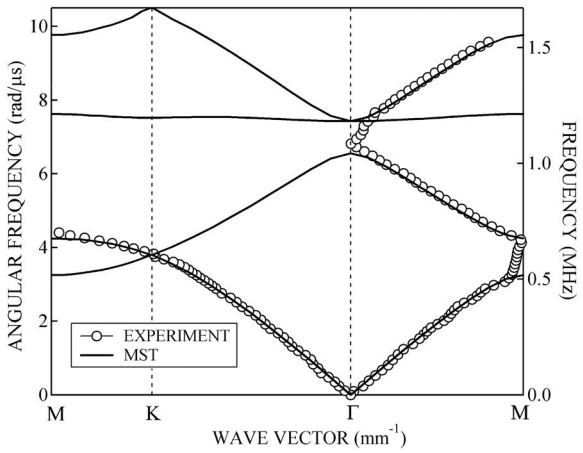

FIG. 1. Comparison of the calculated and measured band structures. Note the absence of the data points corresponding to the modes in the second band along the ΓK direction due to their noncoupling nature.

It is also worthwhile noting that modes in the second band along the ΓK direction have symmetry different from the symmetry of the incident plane wave and therefore cannot couple to a normally incident input pulse in a transmission experiment. The second band along the ΓK direction, which extends from 0.6 to 1.0 MHz, is therefore an example of a *deaf* band.[14,15]

The MST predicts the existence of circular equifrequency contours in the second band. The importance of the circular shape of the equifrequency contours in imaging will be discussed later. The range of frequencies over which the contours are circular can be estimated from the band structure by calculating the percentage deviation of the magnitude of the wave vector along the ΓM direction with respect to the wave vector along the ΓK direction. The deviation as a function of frequency is shown in Fig. 2. One can see that the equifrequency contours are virtually circular for almost the entire second band, except for the narrow range of frequencies below the frequency of 0.69 MHz, at which the wave vectors deviate by 1%. In the following two sections we present and discuss the results of negative refraction and focusing experiments with the crystals described above.

III. NEGATIVE REFRACTION EXPERIMENTS

The group velocity $\vec{v}_g$ (and hence the direction of energy propagation) of sound waves inside the crystal is given by

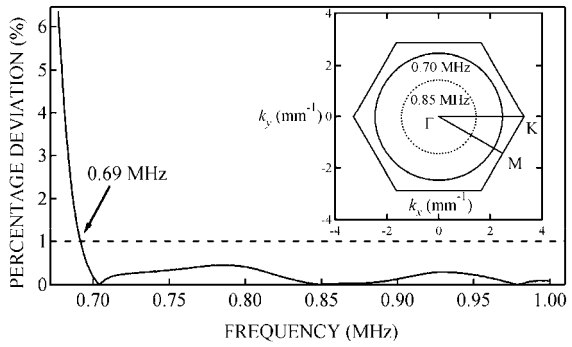

FIG. 2. Estimation of the circularity of the equifrequency contours in the second band.

the gradient of the angular frequency with respect to the wave vector, i.e., $\vec{v}_g = \nabla_{\vec{k}}\omega(\vec{k})$, and is always perpendicular to the equifrequency contours. The circular shape of the equifrequency contours in the second band implies that at this frequency range the wave vector and group velocity are antiparallel *irrespective* of the direction of propagation inside the crystal. It is this property of the equifrequency contours that enables negative refraction of ultrasound to be achieved in our crystal. When a pulse is incident normally on a crystal surface, the wave enters the crystal without any change in its original direction, just as it would do in the case of a prism made out of a regular material (with normal refractive properties). However, for the second band of the phononic crystal, the ensuing wave inside the crystal will have its wave vector opposite to the direction of the propagation $\vec{v}_g$. Therefore when the wave has traveled through the prism, this wave will be incident obliquely on the output side of the crystal and must be refracted upon crossing the crystal-water interface according to Snell's law. In the case of our phononic crystal, it was expected to refract negatively, whereas in the case of a prism made of a regular material, positive refraction should occur. Therefore by recording on which side of the normal the outgoing wave appears as it leaves the crystal, we were able to observe *directly* whether or not negative refraction of the sound waves occurs.

Figure 3 displays snapshots of the output fields at representative frequencies of 0.85 and 0.75 MHz. Additional information on the dynamics of negative refraction can be seen in movies of the output fields.[16] At the frequency of 0.85 MHz, the outgoing pulse is refracted negatively [Fig. 3(a)]. It is interesting to note that at 0.75 MHz, both negatively and positively refracted outgoing pulses were observed [Fig. 3(b)]. The origin of the positively refracted pulse will be discussed later on in this section.

The refraction angle α can be easily calculated with the help of Snell's law,

$$k_{wat}\sin(\alpha) = k_{cr}\sin(60^\circ), \tag{1}$$

where k_{wat} is the wave vector in water and α is the refraction angle. The magnitude of the wave vector inside the first Brillouin zone of the crystal k_{cr} was calculated using the MST. Excellent agreement is observed between measured and predicted refraction angles, as is evident from Table I, which summarizes the results at several different frequencies.

The positively refracted beam at the frequency of 0.75 MHz can be seen to arise from the 1D periodicity of the crystal's surface. Due to this periodicity, the component of the wave vector parallel to the crystal surface $k_\parallel$ can assume any of the values differing from each other by an integer number of surface reciprocal vectors $\vec{g}_s$, i.e., $\vec{k}_\parallel + n\vec{g}_s$, where n is an integer number and $g_s = 2\pi/a_s$ with a_s equal to the surface period. Different parallel components $k_\parallel$ will then

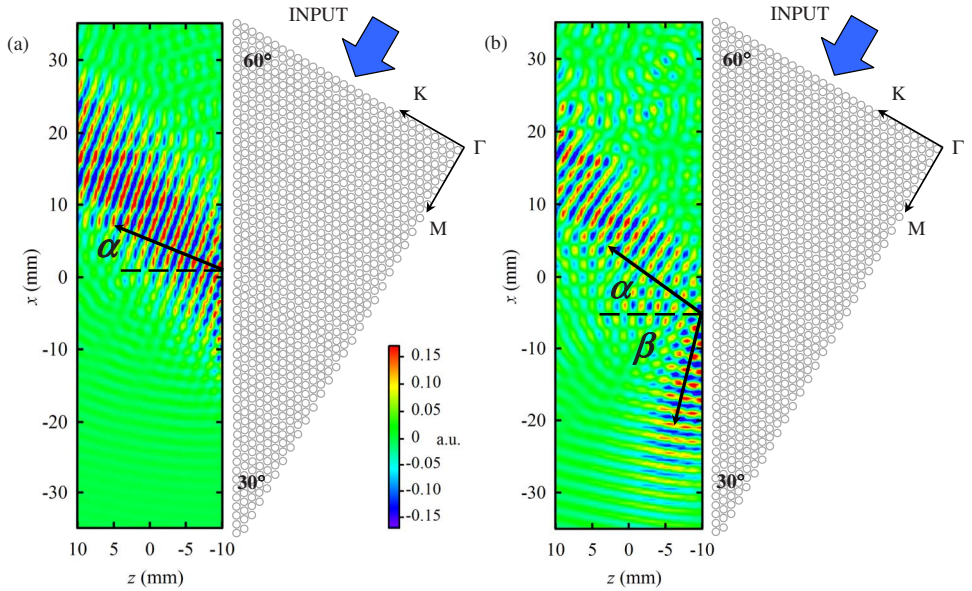

FIG. 3. (Color online) Two snapshots of the outgoing pulses in the negative refraction experiment, obtained by digitally filtering original pulses at the frequency of (a) 0.85 MHz and (b) 0.75 MHz. The crystal position is also indicated with the crystal surface located at the plane $z=-11$ mm. The color scale is in arbitrary units.

TABLE I. Comparison between experimentally measured and theoretically calculated negative angles of refraction. Magnitudes of the wave vectors k_{cr} and k_{wat} are in mm^{-1}.

Frequency (MHz)	k_{cr}	k_{wat}	Refraction angle α	
			Predicted (deg)	Measured (deg)
0.75	2.10	3.16	34.0	34.0±1
0.85	1.40	3.58	20.4	21.0±1
0.90	1.10	3.80	15.0	16.0±1
0.95	0.82	4.01	10.2	10.5±1
1.00	0.50	4.22	6.0	6.0±1

produce beams in water refracted at different angles provided that the condition $k_{\|} < k_{wat}$ holds, since otherwise no transmission to water can occur. In the particular case displayed in Fig. 3(b), Snell's law assumes the following form:

$$k_{wat}\sin(\beta) = g_{\Gamma M} - k = 2\pi/a - k_{cr}\sin(60^\circ), \qquad (2)$$

where $g_{\Gamma M}$ denotes a reciprocal vector along the longest side of the prism-shaped crystal, which is perpendicular to the ΓM direction, and $a_s = a$ along this side. Equation (2) is schematically explained in Fig. 4. From Eq. (2) one finds the value of the refraction angle β of 81°, whereas from Fig. 3(b) the angle β is measured to be 82°±1°. Note also that the combination of $g_{\Gamma M}$ and $k_{\|}$ given by Eq. (2) is the only one that allows transmission to the water, as all other combinations produce parallel wave vectors exceeding the magnitude of the wave vector in water at the frequency of 0.75 MHz.

An alternative explanation of the appearance of the positively refracted pulse can be provided by taking into account that the Bloch wave inside the phononic crystal may be described as a superposition of an infinite number of plane waves. The plane waves, which compose the Bloch wave

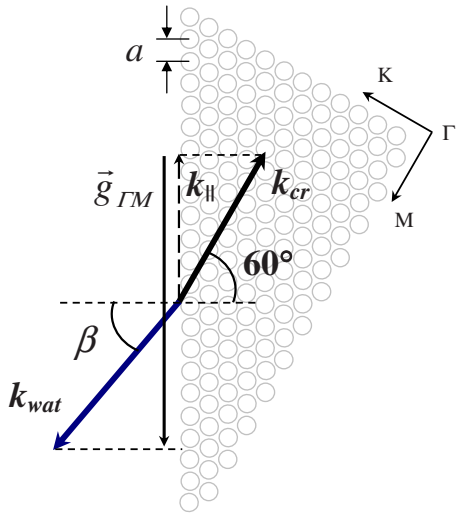

FIG. 4. (Color online) The origin of the positively refracted pulse at 0.75 MHz.

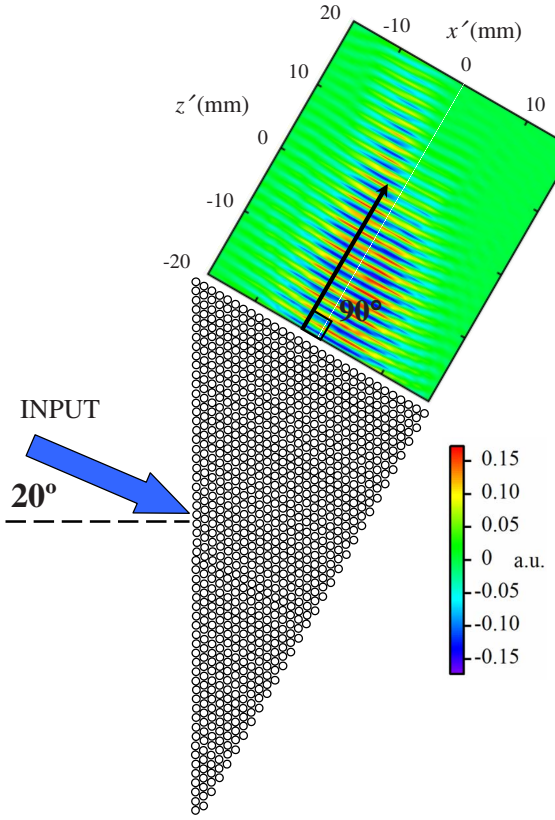

FIG. 5. (Color online) Outgoing pulse in the inverse negative refraction experiment filtered at 0.85 MHz. The color scale is in arbitrary units.

propagating inside the crystal along the ΓM direction, have wave vectors that differ from one another by an integer number of reciprocal lattice wave vectors g_1. In particular, if we consider the wave vector in the second Brillouin zone $\vec{k}_{ext} = \vec{k}_{cr} + \vec{g}_1$, then, with $\vec{k}_{cr}$ negative (opposite to $\vec{v}_g$), $\vec{k}_{ext}$ is parallel to $\vec{v}_g$ and hence to the direction of energy propagation along ΓM. Here $g_1 = 4\pi/\sqrt{3}a = 5.71$ mm^{-1}. Note that k_{ext} belongs to the *extended* zone scheme, while k_{cr} is displayed in the *reduced* zone scheme. When the wave vector k_{ext} is used in Eq. (1) instead of k_{cr}, the same value of the refraction angle β, as predicted by Eq. (2), is obtained. Thus the simplicity of Snell's law is preserved if the refraction is described in terms of k_{ext}, which also corresponds to the largest Bloch wave vector that can couple to the outside medium using Eq. (1). Of course, both descriptions are mathematically identical. The description in terms of the extended zone scheme, however, might be physically more appealing since k_{ext} corresponds to the cumulative phase that is measured in a transmission experiment through a flat phononic crystal and associates positive refraction with a positive wave vector inside the phononic crystal.

To demonstrate negative refraction even more convincingly, we performed an experiment that is the *inverse* of the previous one, with the ultrasound generator and receiver switched and the input pulse incident on the longest side of the crystal, as displayed in Fig. 5. The angle of incidence was chosen to be 20°, which is very close (see Table I) to the

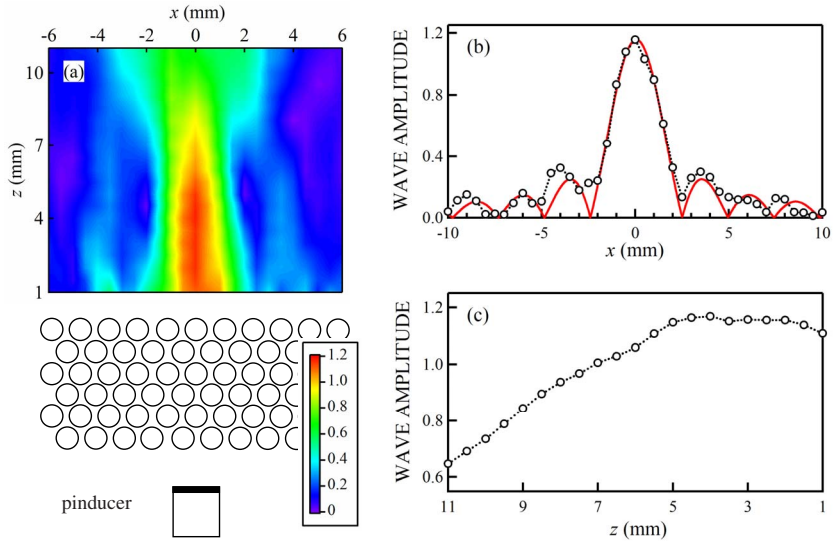

FIG. 6. (Color online) The experiment on imaging the field of the pinducer at 0.70 MHz with a flat phononic crystal filled with and immersed in water. (a) 2D image plot of the wave field amplitude. The color scale shows the normalized amplitude as described in the text. (b) Field profile obtained from the image plot by plotting the amplitude along the x direction at $z=2.9$ mm (open circles connected with a dashed line) and fit of the absolute value of the sinc function (red solid line). (c) Field profile obtained from the image plot by plotting the amplitude along the z direction at $x=0$ mm.

refraction angle at which the 0.85 MHz waves emerged in the direct experiment. Naturally, one would expect the incident pulse to refract negatively into the crystal, propagate through and emerge normally at the shortest side. The experiment is "inverse" in the sense that the pulse follows an *inverse* path as compared to the path of the input pulse in the first experiment. The snapshot of the output field at the frequency of 0.85 MHz is shown in Fig. 5. In agreement with our predictions, the ultrasound pulse was observed to emerge normally to the crystal surface. At other frequencies in the second band, the negatively refracted pulse will be incident *obliquely* at the crystal-water interface and should undergo negative refraction again, which was observed in the experiment. Again, excellent agreement was found between the refraction angles measured for the outgoing beam and theoretical predictions based on the MST equifrequency contours.

At the end of the section on negative refraction, it is worthwhile mentioning that we also performed an experiment similar to the one shown in Fig. 3, but at the frequency corresponding to the first band (namely, 0.25 MHz). In the first band, $\vec{v}_g$ and the wave vector inside the crystal are parallel to each other, since equifrequency contours increase with the increasing wave vector and one expects an outgoing pulse to refract positively through the crystal-water interface. In complete agreement with our expectations, we observed a single positively refracted pulse.

IV. IMAGING WITH FLAT PHONONIC CRYSTALS

Negative refraction must enable a flat phononic crystal to focus sound fields of point sources, since each pair of emitted rays having positive and negative angles of incidence with the same magnitude should refract negatively twice while traveling through the crystal, and be bent back towards a common point on the far side of the crystal. In this section we present experimental verification of this theoretical prediction and examine the image resolution that can be achieved with such a crystal.

In the first imaging experiment, we focused the field emitted by the pinducer using the six-layer flat phononic crystal (see Sec. II for the description of both the crystal and the source). The pinducer was positioned 2.5 mm away from the crystal surface. The amplitude map of the output field at 0.70 MHz, as well as field profiles along the directions parallel and perpendicular to the crystal surface, are shown in Fig. 6. In this figure, the image plot is normalized relative to the value of the pinducer field amplitude that was measured in the absence of the crystal at the position of the maximum of the focal spot.

A clear focusing pattern is observed, as is evident from Fig. 6(a). The full width Δ of the amplitude peak along the x direction was estimated by fitting the data by a sinc function $|\sin(ax)/ax|$, which is appropriate for describing the shape of the image in a 2D experiment. According to the Rayleigh criterion, the resolution is half the full width of the amplitude peak. We found Δ to be 4.9 mm, which corresponds to a resolution of 1.15λ, where λ is the ultrasound wavelength in water. While being narrow along the direction parallel to the crystal surface (x), the observed focal spot is very broad along the perpendicular direction (z). This is expected since at the frequency of 0.70 MHz the equifrequency contours in the crystal and in water do not match, i.e., $k_{cr} \neq k_{wat}$. As a result, the distance between the focus for each pair of rays incident at $\pm\theta_{in}$ and the crystal surface depends on the angle of incidence and thus a focal spot elongated along the z direction is produced. The mismatch between the equifrequency contours also degrades the resolution of the image. In

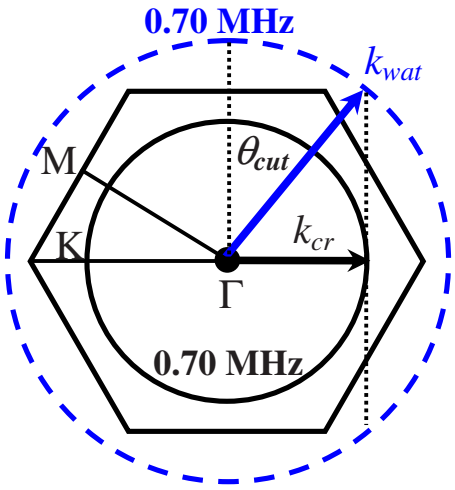

FIG. 7. (Color online) A schematic diagram explaining the origin of the cutoff angle.

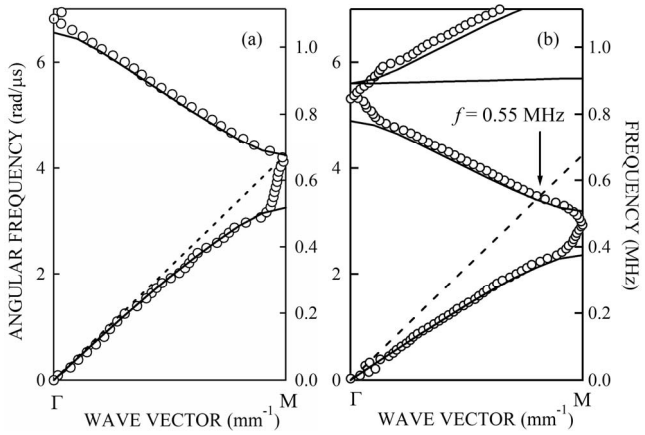

FIG. 8. Comparison of the band structure along the ΓM direction for the water-filled (a) and methanol-filled (b) phononic crystals. As in Fig. 1, the experimental data are represented by open circles and the MST predictions by solid curves. The dispersion relation for water is indicated by the dashed line and can be seen to intersect the second band of the methanol-filled crystal at 0.55 MHz.

our case $k_{cr} < k_{wat}$ and the mismatch introduces a certain cutoff angle θ_{cut}, such that, for any angle of incidence larger than the cutoff angle, incident waves cannot couple to any mode inside the crystal and therefore are not used in the image restoration on the output side of the crystal (see Fig. 7). At the frequency of 0.70 MHz, k_{cr}=2.47 mm^{-1}, which implies a cutoff angle θ_{cut}=56.8°.

The equifrequency contour at 0.70 MHz is the largest circular contour in the second band. (It can be seen from Fig. 2 that at this frequency wave vectors along the ΓM and the ΓK directions deviate from each other by less than 1%). However, this equifrequency contour is still smaller than the corresponding contour in water. Therefore in order to produce an image confined along both the x and z directions as well as to improve image resolution, we designed another phononic crystal, which was similar to the previous one but allowed the liquid inside the crystal to be different from the outside medium (water in our case). The two liquids were prevented from mixing by stretching a very thin (0.01 mm) plastic film over the crystal surface. The negligible influence of the plastic film on transmission through the crystal was confirmed in a separate transmission experiment, in which transmission coefficients through the same crystal (filled with water), with and without the film, were compared. This result is expected, as the film thickness was two orders of magnitude smaller than the sound wavelength in water at the frequency of interest. The new crystal was then filled with methanol, which has speed of sound lower than that in water (1.10 versus 1.49 mm/μs). Qualitatively, one expects that the change of the liquid matrix inside the phononic crystal would simply either stretch or shrink the original band structure along the frequency axis by a factor equal to the ratio of the speeds of sound in the liquids filling the crystal. This qualitative picture was verified by MST calculations and by transmission experiments through the methanol filled crystal, from which the dispersion curve and crystal band structure were determined. A comparison of these results with the calculations and experiments on the water filled crystal is given in Fig. 8, which shows quantitatively the effect on the band structure of reducing the sound velocity in the liquid, and hence also the frequencies of the modes, for the methanol crystal.

The important consequence of changing the liquid inside crystal is to make it possible to find a frequency in the second band of the crystal where the equifrequency contours for the crystal and for water are equal in size. Figure 8(b) reveals the frequency at which this matching condition is met, as it corresponds to the frequency of 0.55 MHz at which the water line intersects the second band of the methanol-filled crystal. Furthermore, the MST calculations confirmed that the shape of this equifrequency contour is indeed circular, with the maximum deviation from a perfect circle being found to be less than 0.4%. Thus the wave vectors were closely matched for all propagation directions. Because the equifrequency contours were matched, *each* incident ray, independent of the angle of incidence, is now coupled to a mode inside the crystal. Thus the AANR regime was achieved. In addition, the angle of refraction equals the angle of incidence for each ray, meaning that *all* rays can be brought to the *same* focal spot on the other side of the crystal. Therefore we can state that the methanol-filled crystal has an *effective* refractive index of −1 at this frequency.

In the first imaging experiment with the methanol-filled crystal, the pinducer was used as a point source. The geometry of the experiment was similar to the one shown in Fig. 6, with the distance between the crystal and the pinducer reduced to 2.0 mm. The input pulse was centered at 0.50 MHz and had a sufficiently broad bandwidth to cover the matching frequency of 0.55 MHz. The amplitude map of the output field at 0.55 MHz, as well as field profiles along the x and z directions, are displayed in Fig. 9. The dramatic improvement of the focal spot shape due to matching equifrequency contours in Fig. 9 is clearly seen when compared to the focal pattern obtained with the water matrix crystal (Fig. 6). The improvement in the shape of the focal

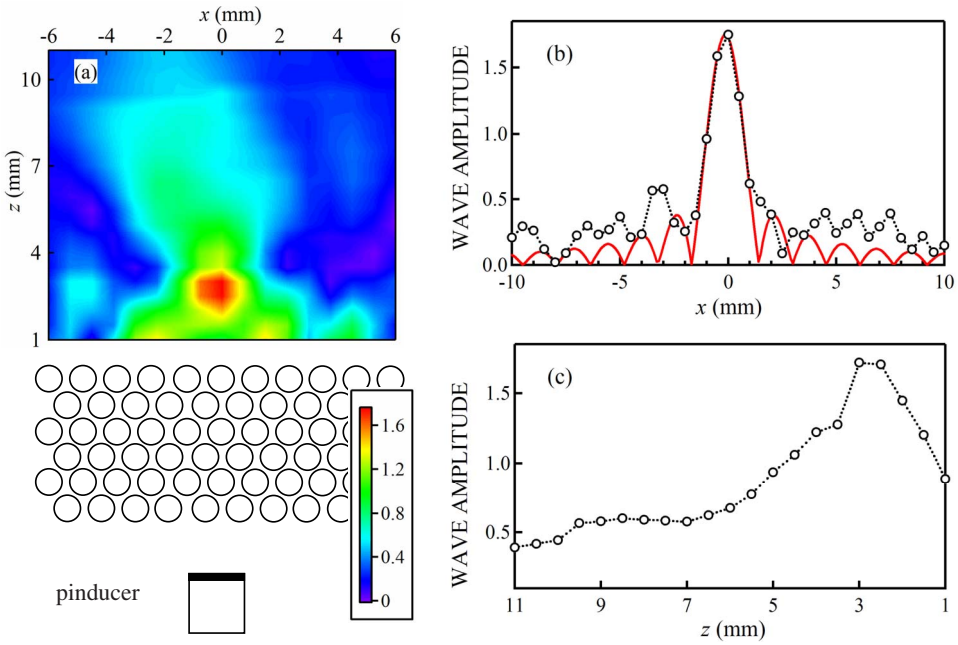

FIG. 9. (Color online) The experiment on imaging the field of the pinducer at 0.55 MHz with a flat phononic crystal filled with methanol. (a) 2D image plot of the wave field amplitude. The amplitude is normalized as in Fig. 6. (b) Field profile obtained from the image plot by plotting along the x direction at $z=2.9$ mm (open circles connected with a dashed line) and fit of the absolute value of the sinc function (red solid line). (c) Field profile obtained from the image plot by plotting along the z direction at $x=0$ mm.

spot along the z direction is especially impressive when compared to the broad field profile in Fig. 6(c) obtained with a water matrix crystal. The extent of the −6 dB region around the focal spot is only 4.2 mm along the z direction for the methanol-filled crystal. Thus by utilizing matching equifrequency contours, the *depth* resolution was significantly improved. Because the regime of AANR was realized, a major improvement of the lateral resolution of the image was also achieved. The width Δ of the amplitude peak in Fig. 9(b) was found to be 3.2 mm, corresponding to a resolution of 0.60λ, which is about two times better than the resolution observed when imaging with the water matrix crystal.

Although the resolution was significantly improved by imaging in the AANR regime, the question about the best possible resolution provided by the system was not resolved by these experiments. In the above experiments, the resolution was limited by the source size, or the pinducer diameter. Recall that the effective pinducer diameter was found to be 2.2 mm. On the other hand, the full width at half maximum (FWHM) of the amplitude peak in Fig. 9(b) was measured to be about 2.0 mm, which is comparable to the pinducer's size. Thus to investigate the true resolution limit, a smaller source must be used. This was accomplished with the line source transducer described in Sec. II. The transducer element was aligned to be parallel with the rods of the methanol matrix crystal and positioned approximately 1.6 mm from the crystal surface. A 2D image plot of the field at the output side of the crystal is shown in Fig. 10. A focal pattern of good quality is obtained with the focal spot clearly seen and narrowly confined both perpendicular and parallel to the crystal surface. From Fig. 10(c), the extent of the −6 dB region along the z axis was found to be 3.8 mm, which is slightly better than the depth resolution observed when the pinducer's field was imaged with the same crystal. Just as in the previous cases, the width of the intensity peak displayed in Fig. 10(b) was measured by fitting the sinc function; in this case the width was found to be 3.0 mm, with a corresponding resolution of 0.55λ. The observed resolution differs by only 10% from the ultimate resolution limit $\lambda/2$ of any conventional imaging system. This difference can be explained by losses or imperfections inside the crystal, which are inevitably present to some degree in any real system. Therefore we demonstrated that the 2D flat phononic crystal with equifrequency contours matched to those of the outside medium is capable of producing images with an excellent resolution approaching the diffraction limit.

Super-resolution (better than diffraction limit) would require the amplification of the evanescent waves. It is clear that no such amplification occurred in our imaging experiments. Luo *et al.*[17] showed that super-resolution can be achieved while imaging with photonic crystals by resonant coupling of the incident evanescent waves to surface photon bound modes, which decay exponentially in both directions away from the surface. For now, it remains an open question whether analogous surface bound states exist in phononic crystals.

V. CONCLUSIONS

Negative refraction of ultrasonic waves was observed at frequencies in the second band of a 2D phononic crystal with circular equifrequency contours. Because of the circular shape of the equifrequency contours, the wave vector inside the crystal and the group velocity are antiparallel for all di-

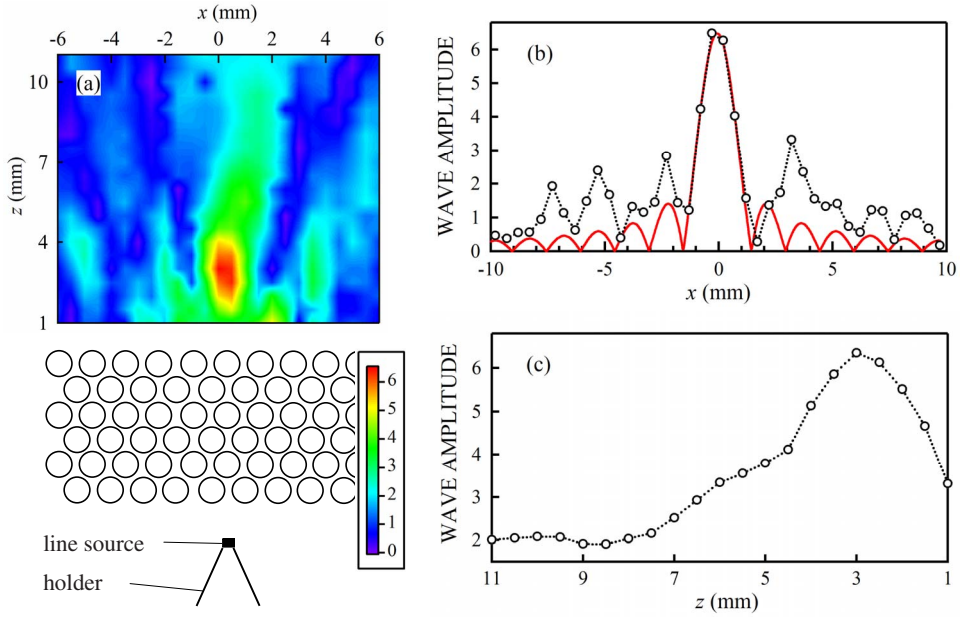

FIG. 10. (Color online) Imaging the field of the line source at 0.55 MHz with a flat phononic crystal filled with methanol. (a) 2D image plot of the wave field amplitude. The amplitude is normalized in the same way as in Fig. 6. (b) Field profile obtained from the image plot by plotting along the x direction at $z=3.0$ mm (open circles connected with a dashed line) and fit of the absolute value of the sinc function (red solid line). (c) Field profile obtained from the image plot by plotting along the z direction at $x=0$ mm.

rections of propagation inside the crystal. The *direct* observation of negative refraction was achieved using a 2D prism-shaped phononic crystal. By scanning the outgoing field with a miniature ultrasound detector, we were able to produce 2D image plots representing snapshots of the negatively refracted pulses as they emerged from the crystal. Our experimental technique also allowed us to monitor the time evolution of the outgoing field, providing direct visualization of the negative refraction phenomenon. Because the acoustic pressure field, not just intensity, is measured in these experiments, the evolution of the actual wave fronts is revealed, allowing the direction of the emerging wave vectors to be directly and accurately determined. The measured refraction angles are in excellent agreement with those predicted by the MST and Snell's law.

Negative refraction also laid the basis for imaging experiments with flat 2D phononic crystals consisting of steel rods immersed in a liquid. The ultrasonic field emitted by a point-like source (a pinducer), which was positioned in front of the crystal, was brought to a focus on the opposite side of the crystal by negatively refracting each incident ray twice. For a water-filled crystal, the focal depth as well as the lateral resolution of the image suffered from the mismatch between corresponding equifrequency contours in the water and inside the crystal. The regime of all angle negative refraction was achieved by designing and building a phononic crystal filled with a liquid (methanol) with a lower sound velocity than the outside medium (water). This resulted in *matching* equifrequency contours at the frequency of 0.55 MHz. By imaging with this crystal, a dramatic improvement in both the resolution and the focal depth of the pinducer's images was observed. The best resolution of 0.55λ was recorded by imaging the field of a *subwavelength* line source (custom-built ultrasonic transducer). The achieved resolution is just above the diffraction limit and is much better than the resolution provided by commercially available focusing transducers. We did not observe any evidence of the amplification of evanescent waves, which is required for achieving resolution better than the diffraction limit.

ACKNOWLEDGMENT

Financial support from NSERC of Canada and from the University of Manitoba Graduate Fellowship Program is gratefully acknowledged.

[1] V. G. Veselago, Usp. Fiz. Nauk **92**, 517 (1964).
[2] J. B. Pendry, Contemp. Phys. **45**, 191 (2004).
[3] R. A. Shelby, D. R. Smith, and S. Shultz, Science **292**, 77 (2001).
[4] M. Notomi, Phys. Rev. B **62**, 10696 (2000).
[5] E. Cubukcu, K. Aydin, E. Ozbay, S. Foteinopoulou, and C. M. Soukoulis, Nature (London) **423**, 604 (2003).
[6] P. V. Parimi, W. T. Lu, P. Vodo, J. Sokoloff, J. S. Derov, and S. Sridhar, Phys. Rev. Lett. **92**, 127401 (2004).
[7] C. Luo, S. G. Johnson, J. D. Joannopoulos, and J. B. Pendry, Phys. Rev. B **65**, 201104(R) (2002).
[8] E. Cubukcu, K. Aydin, E. Ozbay, S. Foteinopoulou, and C. M. Soukoulis, Phys. Rev. Lett. **91**, 207401 (2003).

[9] Z. Lu, J. Murakowski, C. Shuetz, S. Shi, G. Schneider, and D. Prather, Phys. Rev. Lett. **95**, 153901 (2005).
[10] S. Yang, J. H. Page, Z. Liu, M. L. Cowan, C. T. Chan, and P. Sheng, Phys. Rev. Lett. **93**, 024301 (2004).
[11] M. Ke, Z. Liu, C. Qiu, W. Wang, J. Shi, W. Wen, and P. Sheng, Phys. Rev. B **72**, 064306 (2005).
[12] X. Hu, Y. Shen, X. Liu, R. Fu, and J. Zi, Phys. Rev. E **69**, 030201(R) (2004).
[13] J. Mei, Z. Liu, J. Shi, and D. Tian, Phys. Rev. B **67**, 245107 (2003).
[14] J. V. Sánchez-Pérez, D. Caballero, R. Mártinez-Sala, C. Rubio, J. Sánchez-Dehesa, F. Meseguer, J. Llinares, and F. Gálvez, Phys. Rev. Lett. **80**, 5325 (1998).
[15] T. F. Krauss, R. M. De La Rue, and S. Brand, Nature (London) **383**, 699 (1996).
[16] See EPAPS Document No. E-PRBMDO-76-021745 for movies showing the time evolution of the output fields at 0.85 and 0.75 MHz. The experimental geometry is the same as in Fig. 3. For more information on EPAPS, see http://www.aip.org/pubservs/epaps.html.
[17] C. Luo, S. G. Johnson, J. D. Joannopoulos, and J. B. Pendry, Phys. Rev. B **68**, 045115 (2003).